

Modeling time series of microwave brightness temperature at Dome C, Antarctica, using vertically resolved snow temperature and microstructure measurements

L. Brucker, G. Picard, L. Arnaud, J.M. Barnola, M. Schneebeli, H. Brunjail, E. Lefebvre, M. Fily

▶ **To cite this version:**

L. Brucker, G. Picard, L. Arnaud, J.M. Barnola, M. Schneebeli, et al.. Modeling time series of microwave brightness temperature at Dome C, Antarctica, using vertically resolved snow temperature and microstructure measurements. Journal of Glaciology, 2011, 57 (201), pp.171-182. 10.3189/002214311795306736 . insu-00646667

HAL Id: insu-00646667
https://insu.hal.science/insu-00646667

Submitted on 23 Nov 2021

HAL is a multi-disciplinary open access archive for the deposit and dissemination of scientific research documents, whether they are published or not. The documents may come from teaching and research institutions in France or abroad, or from public or private research centers.

L'archive ouverte pluridisciplinaire **HAL**, est destinée au dépôt et à la diffusion de documents scientifiques de niveau recherche, publiés ou non, émanant des établissements d'enseignement et de recherche français ou étrangers, des laboratoires publics ou privés.



Distributed under a Creative Commons Attribution 4.0 International License

Modeling time series of microwave brightness temperature at Dome C, Antarctica, using vertically resolved snow temperature and microstructure measurements

Ludovic BRUCKER,[1] Ghislain PICARD,[1] Laurent ARNAUD,[1] Jean-Marc BARNOLA,[1†] Martin SCHNEEBELI,[2] Hélène BRUNJAIL,[1] Eric LEFEBVRE,[1] Michel FILY[1]

[1] *Laboratoire de Glaciologie et Géophysique de l'Environnement, CNRS/Université Joseph Fourier – Grenoble I, 54 rue Molière, BP 96, 38402 Saint-Martin-d'Hères Cedex, France*
E-mail: lbrucker@lgge.obs.ujf-grenoble.fr
[2] *WSL Institute for Snow and Avalanche Research SLF, Flüelastrasse 11, CH-7260 Davos Dorf, Switzerland*

ABSTRACT. Time series of observed microwave brightness temperatures at Dome C, East Antarctic plateau, were modeled over 27 months with a multilayer microwave emission model based on dense-medium radiative transfer theory. The modeled time series of brightness temperature at 18.7 and 36.5 GHz were compared with Advanced Microwave Scanning Radiometer–EOS observations. The model uses in situ high-resolution vertical profiles of temperature, snow density and grain size. The snow grain-size profile was derived from near-infrared (NIR) reflectance photography of a snow pit wall in the range 850–1100 nm. To establish the snow grain-size profile, from the NIR reflectance and the specific surface area of snow, two empirical relationships and a theoretical relationship were considered. In all cases, the modeled brightness temperatures were overestimated, and the grain-size profile had to be scaled to increase the scattering by snow grains. Using a scaling factor and a constant snow grain size below 3 m depth (i.e. below the image-derived snow pit grain-size profile), brightness temperatures were explained with a root-mean-square error close to 1 K. Most of this error is due to an overestimation of the predicted brightness temperature in summer at 36.5 GHz.

INTRODUCTION

To analyze trends in the Antarctic climate, accurate observations are necessary. These observations cannot be taken only from the current network of meteorological stations, mainly located at coastal sites, due to the sparsity of the stations (Turner and others, 2005; Steig and others, 2009). Remote sensing appears the only way to observe spatially resolved variations in the polar climate.

Among the different spaceborne sensors, microwave radiometers can be used to study the temporal and spatial evolution of the temperature over polar regions, because they have measured the thermal radiation emitted by the snowpack several times per day for more than 30 years. The radiometer measurement, expressed as brightness temperature, T_B, is (in dry snow) mostly related to the vertical distribution of snow temperature and to the vertical profile of snow microstructure properties, such as grain size and density, which govern snow emissivity (Zwally, 1977; Surdyk, 2002).

Efforts to predict snow brightness temperature and emissivity using radiative transfer models driven by snow measurements, such as the dense-medium radiative transfer theory (DMRT) (Tsang and others, 2000), the Microwave Emission Model of Layered Snowpacks (MEMLS; Wiesmann and Mätzler, 1999) and the Helsinki University of Technology (HUT) snow microwave emission model (Pulliainen and others, 1999), are growing both for seasonal snow (e.g. Macelloni and others, 2001; Tedesco and Kim, 2006; Tedesco and others, 2006; Liang and others, 2007; Lemmetyinen and others, 2009) and for perennial snow (Macelloni and others, 2007).

In this study, we model the microwave brightness temperature at Dome C (75°06′ S, 123°21′ E; 3240 m a.s.l.) on the East Antarctic plateau using a model, based on the DMRT, driven by in situ snow temperatures and microstructure profiles. The channels used are 18.7 and 36.5 GHz at vertical and horizontal polarization.

In a previous study, Macelloni and others (2007) computed time series of brightness temperature at Dome C by driving a microwave emission model with snow measurements. The time series of brightness temperature from January to October were modeled with a root-mean-square error (rmse) of 1.18 and 2.7 K at 18.7 and 36.5 GHz, respectively. This relatively high rmse may be explained by the inaccuracy of the snow grain-size profile. Indeed, the snow grain-size profile strongly influences the microwave emissivity (e.g. Wiesmann and others, 1998; Mounirou Toure and others, 2008; Brucker and others, 2010), hence highly resolved and quantitative measurements are crucial to model emissivity accurately. Furthermore, it was shown that an accurate knowledge of the snow grain-size profile is the most important snow property when modeling emissivities in Antarctica at several frequencies (Brucker and others, 2010).

Nevertheless, unlike snow density and temperature, snow grain size is difficult to measure. The definition of grain size is not obvious owing to the wide variety of snow grain shapes found in natural snow (e.g. Colbeck and others, 1990).

Macelloni and others (2007) took the snow grain size as the maximum dimension of the prevalent grains for each snow layer according to Colbeck and others (1990). The grain-size profile was measured by visual inspection using a hand lens and traditional macro photographs of grains. However, traditional methods of direct visual inspection in snow pits lack repeatability, as it is necessary to select

†Deceased.

Downloaded from https://www.cambridge.org/core. 23 Nov 2021 at 12:30:57, subject to the Cambridge Core terms of use.

grains (e.g. Domine and others, 2006). In addition, these measurements do not provide the effective grain size required in radiative transfer modeling (Painter and others, 2007).

A physically more sensible way to define grain size is by specific surface area (SSA) (Giddings and LaChapelle, 1961; Domine and others, 2001), i.e. the total surface area of the air–ice interface per unit mass ($m^2\ kg^{-1}$). The SSA is related to the optical radius, r_{opt} (Grenfell and Warren, 1999):

$$r_{opt} = \frac{3}{\rho_{ice}\,SSA}, \quad (1)$$

where ρ_{ice} is the ice density ($917\ kg\ m^{-3}$).

The SSA of snow can be measured by different methods: in two dimensions by stereology (Perla and others, 1986; Davis and others, 1987; Arnaud and others, 1998; Matzl and Schneebeli, 2010) and in three dimensions by methane adsorption (Legagneux and others, 2002), X-ray tomography (Flin and others, 2003; Barnola and others, 2004; Kerbrat and others, 2008) or snow reflectance in the near and short infrared (Domine and others, 2006; Matzl and Schneebeli, 2006; Painter and others, 2007; Gallet and others, 2009). Whatever the technique used, SSA measurements present the major advantage of being observer-independent. In addition, with the current accuracy of the measurements, the dependence of the reflectance–SSA relationship on the grain shape predicted by several authors (Grenfell and Warren, 1999; Kokhanovsky and Zege, 2004; Picard and others, 2009a) does not seem significant in natural snow (Gallet and others, 2009).

These methods take measurements at one point, except for near-infrared (NIR) photography which allows continuous vertical profiling of SSA with one snapshot. This represents an important advantage over the other techniques in modeling the passive microwave emission, because all the existing models consider snow as a layered medium. Therefore, the NIR photography method is the most convenient for our purpose.

NIR photography (Matzl and Schneebeli, 2006; Langlois and others, 2010) measures the hemispherical directional reflectance over a broad range of wavelengths of ~850–1100 nm, with high spatial resolution (typically a few millimeters). To calculate the vertical profile of SSA from the reflectance measurements, we considered existing relationships both developed from empirical stereological measurements and based on theoretical calculations with radiative transfer models.

In this paper, we use NIR photography to derive SSA, and we use density and temperature profiles measured at high vertical resolution to drive the multilayer (ML) microwave radiative transfer models, DMRT-ML and MEMLS, in order to compute the brightness temperature.

Table 1. Mean and standard deviation, σ, of snow temperatures (K) measured in January 2007 and 2008 with T0 and T1 initially near the surface and at 0.1 m depth respectively

Probe	January 2007		January 2008	
	Mean	σ	Mean	σ
T0	244.95	6.94	243.69	3.45
T1	242.94	3.72	242.33	2.28

METHODS

Microwave data

Microwave observations were acquired at 18.7 and 36.5 GHz by the Advanced Microwave Scanning Radiometer – Earth Observing System (AMSR-E). The daily-averaged brightness temperatures were extracted from the 'AMSR-E/Aqua Daily L3 12.5 km Brightness Temperature, Sea Ice Concentration, and Snow Depth Polar Grids' dataset provided by the US National Snow and Ice Data Center (NSIDC), with a spatial resolution of 12.5 km × 12.5 km. According to the AMSR-E webpage (http://nsidc.org/data/docs/daac/AMSR-E__instrument.gd.html), the total sensor bias error is 0.66 K at 100 K and slightly changes with temperature to 0.68 K at 250 K.

The dataset contains, for each day, the average of the daily-averaged ascending orbits and daily-averaged descending orbits. At Dome C, due to the sun-synchronous near-polar orbit, there are typically seven passes per day between 1400 and 0000 h, local time.

Measurements of snow properties

Snow temperature

Snow temperature profiles were recorded every hour (from November 2006), down to 21 m, with 35 probes. The temperature probes were located ~1 km to the west of the Concordia station and 15 m from the snow pit where the density and NIR reflectance were measured. Initially, in the top 2 m of the snowpack, there were 14 probes (every 0.1 m down to 0.6 m depth then every 0.2 m down to 2 m). All probes were intercalibrated with a relative accuracy of ±0.01 K; the absolute precision is ±0.03 K.

To accurately model the microwave radiation emitted by the snowpack, the absolute depth of the temperature probes and their burying with time need to be known. To estimate the annual amount of snow accumulated above the temperature probes, the daily variations of snow temperatures in January 2007 and January 2008 were compared. These variations are related to the 24 hour cycle of solar radiation and they exponentially decrease with increasing depth (Brandt and Warren, 1997).

In January 2007, temperature probe T0 was set near the surface and T1 was set 0.1 m below the surface. Mean and standard deviation of snow temperatures measured in January 2007 and 2008 by the T0 and T1 probes are reported in Table 1. The standard deviation measured with T1 in 2007 (3.72 K) is similar to that measured with T0 (3.45 K) 1 year later (Table 1).

From this, we estimated snow accumulation above the sensors to be ~0.1 m between January 2007 and 2008. Such an accumulation is in agreement with measurements at Dome C (Urbini and others, 2008). For the model we therefore assume that the snow temperature probes were buried at a constant rate of $0.1\ m\ a^{-1}$ with respect to the initial depths in January 2007.

To compare the modeled brightness temperatures at the time of the satellite observations, we averaged the 2 hourly profile of temperatures between 1400 and 0000 h local time and used this averaged value.

Snow density

Snow density was measured in December 2006 in a snow pit, from the surface down to 3 m depth, with 2–3 cm vertical

Downloaded from https://www.cambridge.org/core. 23 Nov 2021 at 12:30:57, subject to the Cambridge Core terms of use.

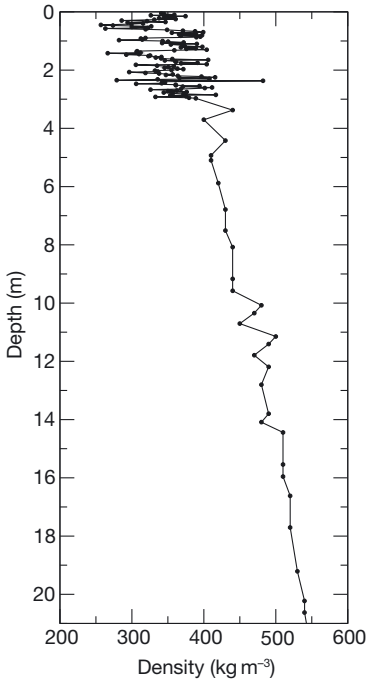


Fig. 1. Snow density profile measured at Dome C, used to drive the DMRT-ML model. From 0 to 3 m depth, snow density was measured in a snow pit with a 2–3 cm vertical resolution. Below 3 m, measurements were made on a snow core. See Figure 2 for details of the top 3 m.

resolution. Below 3 m, the density was measured in a snow core down to 21 m depth, every 0.5–1 m (Figs 1 and 2a). Mean snow density of the top 3 m was 350 kg m^{-3} and increased to 550 kg m^{-3} at 21 m.

Snow grain size

The snow grain-size profile was derived from NIR reflectance measured by photography. The method was adapted from Matzl and Schneebeli (2006). Three NIR photographs were taken to cover a 0.6 m wide and 3 m deep snow pit wall (Fig. 2b). To convert pixel intensity to reflectance, ω, eight panels of two target references (Spectralon 50% and 99%) were evenly distributed on the snow wall. All the measurements were made under diffuse light conditions. The camera was a modified Canon 400D for NIR photography in the wavelength range 850–1100 nm, with a fixed zoom lens (EF 24 mm, f= 2.8).

After the photography, snow samples were taken from the wall of the snow pit for stereological measurements of the SSA to establish a relationship between NIR reflectance and SSA (Brunjail and others, 2009). The following empirical relationship is based on eight stereological measurements collected at Dome C, referred to hereafter as DC:

$$\mathrm{SSA} = 0.0034\mathrm{e}^{9.901\omega}. \quad (2)$$

However, as only a few measurements are available from DC, we also use two other relationships. The first is the combined set from the European Alps (Matzl and Schneebeli, 2006) and Dome C (referred to hereafter as ADC):

$$\mathrm{SSA} = 0.0397\mathrm{e}^{7.046\omega}. \quad (3)$$

For the DC and ADC relationships, the unit of SSA was converted from m^{-1} to m^2 kg^{-1} by dividing by the ice density. The latter relationship is based on a theoretical

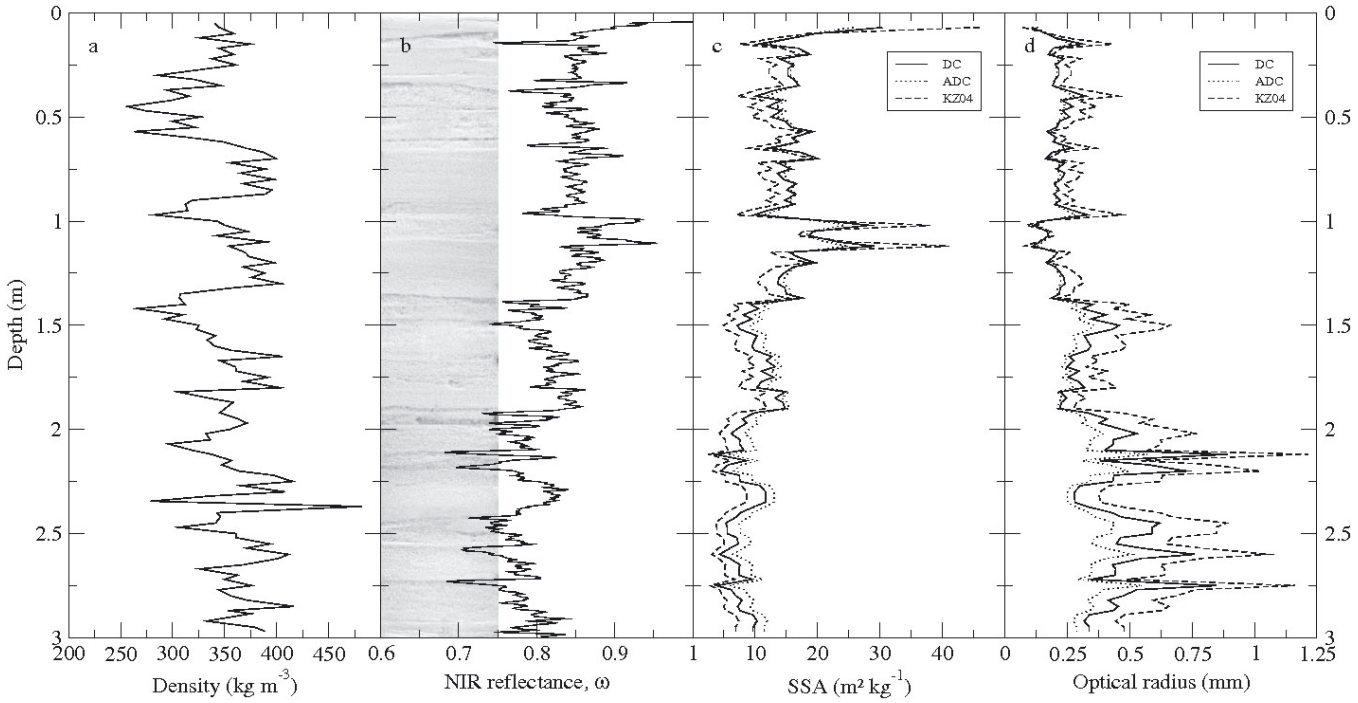


Fig. 2. Profiles of measured snow microstructure properties down to 3 m depth. (a) Snow density, (b) NIR photograph of the snow pit wall and NIR reflectance, ω, (c) specific surface area of snow derived from the three relationships (DC, ADC and KZ04) and (d) derived optical radius computed from the three SSA profiles and Equation (1).

Downloaded from https://www.cambridge.org/core. 23 Nov 2021 at 12:30:57, subject to the Cambridge Core terms of use.

model (Kokhanovsky and Zege, 2004) adapted by Picard and others (2009a) (referred to hereafter as KZ04):

$$\mathrm{SSA} = b^2\gamma\frac{486}{49\rho_{\mathrm{ice}}\log(\omega)^2}. \quad (4)$$

The ice absorption coefficient, γ, is given by:

$$\gamma = 2k\,n_{\mathrm{ice}} = \frac{4\pi}{\lambda}1.34\times10^{-7}, \quad (5)$$

where k is the wavenumber and n_{ice} is the imaginary part of the ice refraction index taken from Warren and Brandt (2008). γ was computed at a wavelength, λ, of 850 nm, assuming this is the dominant wavelength under natural light. KZ04 refers to the factor b that depends solely on snow grain shape (Picard and others, 2009a), but it is unknown for natural snow. The possible range of b values estimated by theory is 3.39–4.07, corresponding to perfectly cubic and spherical grains, respectively (Picard and others, 2009a).

There is much observational evidence that grain shapes can be various and complex in Antarctica; but most of the grains at Dome C are of two types, either coarse and faceted with few rounded parts, or small rounded grains initially present in hard packed snow which have then evolved toward slightly faceted grains. Cup-like or elongated grains are rare. Since the mixture of plane faces and rounded parts dominates, we used a shape factor $b = 3.7$, intermediate between that of spheres and cubes.

The three relationships between NIR reflectance and SSA (DC, ADC and KZ04) were used to calculate the SSA profile. DC, ADC and KZ04 all show the same trend in SSA; the difference is ~30% (Fig. 2c). Averaged SSA values over the profile are 12, 13 and 9.8 $\mathrm{m^2\,kg^{-1}}$ for DC, ADC and KZ04, respectively. The theoretical KZ04 relationship gives the lowest values of SSA.

These three relationships are used to study the validity of the method to model brightness temperature. We do not attempt to explain the difference between them.

Currently, few SSA measurements are available in Antarctica, even at Dome C. Nevertheless, the variations in SSA derived from the NIR photographs are in agreement with those measured by Gallet and others (2010), ranging from 38 to 14 $\mathrm{m^2\,kg^{-1}}$ from the surface to 0.7 m depth, with the DUal-Frequency Integrating Sphere for Snow SSA (DUFISSS; Gallet and others, 2009), a dedicated probe.

Figure 2b shows that ω had a decreasing trend with depth, corresponding to a decrease in SSA (Fig. 2c) and a corresponding increase in optical radius (Fig. 2d). Since no NIR photograph was acquired below 3 m depth, a constant SSA of 9.8 $\mathrm{m^2\,kg^{-1}}$ was assumed below this depth. This value was measured at 4 m depth on a snow core using the stereological method. The limit of this assumption is evaluated in the 'Results and discussion' section.

Snow microwave emission modeling

To predict microwave brightness temperature, we used a multilayer electromagnetic model (DMRT-ML) based on the DMRT (Tsang and Kong, 2001). This theory has been extensively applied, in single and multilayered configurations, to study active and passive remote sensing of both seasonal and perennial snow (e.g. Tsang and others, 2000; Macelloni and others, 2007; Tsang and others, 2007; Grody, 2008; Liang and others, 2008) as well as snow over sea ice (e.g. West and others, 1993).

The model assumes that snow is composed of ice spheres. The effective dielectric constant is solved using the first-order quasi-crystalline approximation and the Percus–Yevick pair distribution for non-sticky grains, i.e. grains which do not form aggregates (Tsang and Kong, 2001). The computation is valid in the limit of low frequency and small sphere radius, r (i.e. $2\pi r/\lambda < 1$).

DMRT is in agreement with numerical solutions of the Maxwell equations in three-dimensional simulations (NMM3D-DMRT) up to a density of ~275 kg $\mathrm{m^{-3}}$ (Liang and others, 2006; Tsang and others, 2008). However, this is lower than the typical density of snow at Dome C.

The propagation of the radiation through the snowpack is computed using the discrete-ordinate radiative transfer (DISORT) method (Jin, 1993). DMRT-ML accounts for multiple scattering between layers. The layers are plane parallel and thicker than the wavelength, so interferences due to multiple reflections are negligible. The thickness of the snow layer ranges, in this study, between 0.02 and 1 m. Each layer is fully characterized by thickness, radius of sphere, density and temperature.

To avoid model-dependent results, MEMLS (Wiesmann and Mätzler, 1999) was also used. This model is based on a radiative transfer using the six-flux theory to describe multiple volume scattering and absorption. In our study, the parameterization of the scattering coefficient is based on the improved Born approximation (Mätzler, 1998; Mätzler and Wiesmann, 1999). The input variables are similar to those used by DMRT-ML, except the grain size. Indeed, MEMLS requires the exponential correlation length, p_{exp}, to quantify the grain size. Correlation length, p_c, is theoretically related to optical diameter and density (Debye and others, 1957):

$$p_c = \frac{4}{3}(1-f)r_{\mathrm{opt}}, \quad (6)$$

where f is the fractional volume. Mätzler (2002) explains that while p_{exp} is different from p_c, these two variables are related by a multiplicative parameter. In this study, we used Equation (6) as a basis.

Atmospheric microwave emission modeling

The snow microwave emission model computes top-of-snowpack brightness temperature. To predict satellite observations at the top of the atmosphere, atmospheric attenuation and emission due to water vapor and gas constituents need to be accounted for (Rosenkranz, 1992). These were evaluated using the radiative model, RTTOV-9.1 (Saunders and others, 1999) driven by the temperature and water vapor concentration profiles extracted from European Centre for Medium-Range Weather Forecasts (ECMWF) ERA-40 meteorological reanalysis (Uppala and others, 2005).

RESULTS AND DISCUSSION

Direct modeling with measured snow grain-size profile

In this section, we assume that the optical radius derived from the SSA measurements (using the DC relationship) is able to represent the radius of spheres in DMRT-ML. We therefore directly use the optical radius profile as input to DMRT-ML. Figure 3a shows the modeled and observed time series of brightness temperature. Modeling results are greatly overestimated at both frequencies by ~28 K. In addition, the

Downloaded from https://www.cambridge.org/core. 23 Nov 2021 at 12:30:57, subject to the Cambridge Core terms of use.

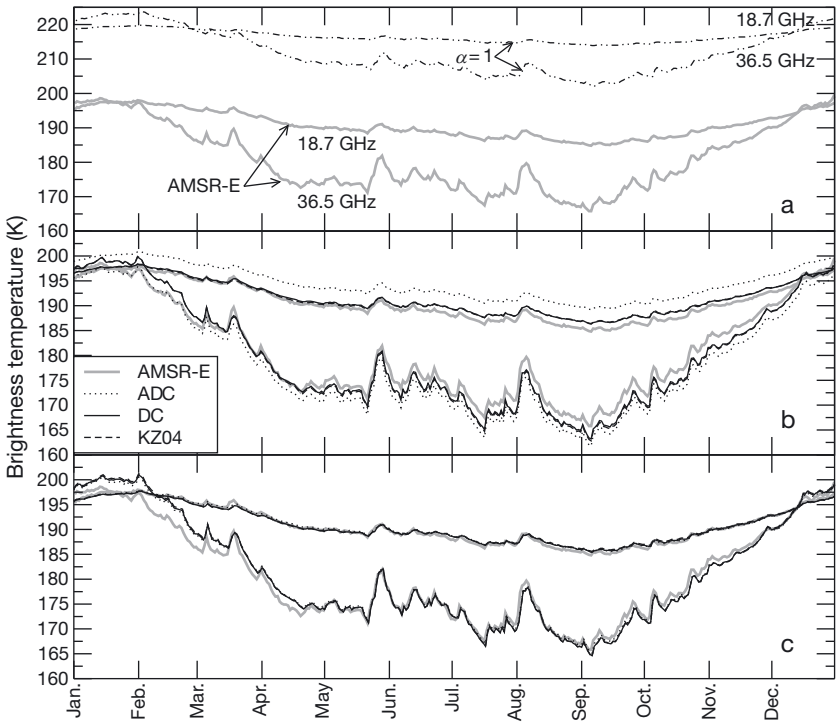


Fig. 3. Observed (gray curves) and modeled time series of vertically polarized brightness temperature at Dome C in 2007 at 18.7 and 36.5 GHz using: (a) DC and $\alpha = 1$, (b) the three relationships (DC, ADC and KZ04) with a calibrated α (Table 3) and (c) the three relationships with a calibrated α and a calibrated snow grain size below 3 m depth (Table 4).

predicted amplitudes of the annual cycle are weaker than in the observations. For instance, at 36.5 GHz the predicted amplitude is 20 K whereas the observed amplitude of the annual cycle is 30.1 K. The results are similar for the two other relationships, ADC and KZ04.

In theory, the amplitude of the time series (i.e. the dynamic range of the brightness temperature) decreases with a decreasing extinction coefficient (Surdyk, 2002). Since the extinction coefficient is the sum of the scattering coefficient, K_s, and the absorption coefficient, K_a, the underestimation of the amplitude may be explained by an underestimation of either K_s or K_a.

Further, in theory, the emissivity increases with K_a but decreases with K_s. Hence, the overestimation by the model of the mean brightness temperature results from an overestimation of the emissivity, caused by a too low K_s, or a too high K_a.

Therefore, the only explanation for both the underestimation of the amplitude and the overestimation of the mean brightness temperature is that K_s is underestimated. Since K_s is mainly driven by grain size, we conclude that the sphere radius relevant for microwave calculations is larger than the optical radius (which is relevant for optical calculations).

In addition, the values of K_s (Table 2), both at 18.7 and 36.5 GHz, are much lower than those obtained by measurements (Wiesmann and others, 1998) and modeling (e.g. Chen and others, 2003) for dry snow. In contrast, the absorption coefficients of $\sim$0.057 m^{-1} at 18.7 GHz, and 0.220 m^{-1} at 36.5 GHz (Table 2), are reasonable for dry snow for densities close to 350 kg m^{-3} (Wiesmann and others, 1998). This further confirms that K_s is underestimated.

It is also worth noting that in the DMRT the absorption coefficient is independent of grain size. Hence, modifying the snow grain-size profile does not change K_a.

Simulations were repeated with MEMLS and the results show that modeling the brightness temperatures with the measured snow grain-size profile results in a large overestimation at both frequencies, as with DMRT-ML. In addition, the scattering and absorption coefficients are of the same order as those obtained with DMRT-ML.

In conclusion, several arguments support the fact that the deficiency of the models comes from an underestimation of the scattering coefficient due to an underestimation of the grain size.

Calibrated snow grain-size profile

The optical radius profile was scaled by a factor α to drive DMRT-ML, according to:

$$r^{\mathrm{DMRT}} = \alpha\, r_{\mathrm{opt}}. \tag{7}$$

It is worth noting that the use of such a scaling factor does not change the vertical gradient of the grain-size profile.

The value of α was found by minimizing the mean rmse between the observed and modeled time series of brightness

Table 2. Values of scattering and absorption coefficients (m^{-1}) averaged over 0–3 m directly modeled by DMRT-ML with the measured snow grain-size profile ($\alpha = 1$) and the calibrated snow grain-size profile ($\alpha = 1.9$)

	18.7 GHz	36.5 GHz
K_s ($\alpha = 1$)	0.03	0.48
K_s ($\alpha = 1.9$)	0.22	3.26
K_a	0.057	0.22

Downloaded from https://www.cambridge.org/core. 23 Nov 2021 at 12:30:57, subject to the Cambridge Core terms of use.

Table 3. Estimated scaling factor, α, and rmse (K) between observed and modeled brightness temperature, in 2007 for the three relationships, DC, ADC and KZ04. The snow grain size below 3 m depth was fixed at SSA = 9.8 m^2 kg^{-1}; the equivalent $r^{z>3m}$ is given for all cases

Relationship	α	$r^{z>3m}$	$rmse_{18.7}$	$rmse_{36.5}$	rmse
DC	2.50	0.83	0.94	1.76	1.41
ADC	2.85	0.95	3.60	2.95	3.29
KZ04	1.89	0.63	0.94	1.96	1.54

temperature, T_B^{AMSR-E} and T_B^{mod}, respectively, at frequency ν, using the Nelder–Mead simplex method (Lagarias and others, 1998). We define $rmse_\nu$ as:

$$rmse_\nu = \sqrt{N^{-1}\sum_i^N \left(T_{B\nu,i}^{AMSR-E} - T_{B\nu,i}^{mod}\right)^2}, \quad (8)$$

where N is the number of days when both valid satellite observations and temperature records were available (N = 345 in 2007). The mean rmse was then calculated:

$$rmse = \sqrt{0.5(rmse_{18.7}^2 + rmse_{36.5}^2)}. \quad (9)$$

The minimization gives α equal to 2.50, 2.85 and 1.89 for the DC, ADC and KZ04 relationships, respectively. As expected, $\alpha \gg 1$ and the α values significantly increase the grain sizes initially derived from NIR photographs. The reasons why $\alpha \gg 1$ can be divided into four classes:

DMRT-ML assumes non-sticky grains, which may be incorrect for snow because it is a sintered material. By considering sticky spheres (Tse and others, 2007), values of α up to 4 can be obtained, depending on the stickiness parameter (Tsang and Kong, 2001). We did not consider stickiness in our study because, as yet, there is no rigorous way to evaluate it. However, the values of α obtained by optimization (1.89–2.85) may be an indirect evaluation of the stickiness parameter.

Another significant assumption is the use of a single radius per snow layer although snow grain size is usually distributed over a large range. Several studies (e.g. Jin, 1993; West and others, 1993) noted the influence of a distribution in grain size, since large grains scatter much more than small grains in the low-frequency limit (Jin, 1993). In particular, it was shown that the scattering efficiency produced by a snow layer with a Rayleigh distribution of grain sizes can be modeled considering a single grain size ~1.4 times larger than the mean snow grain size of the distribution (Jin, 1993).

α also allows us to compensate for potential uncertainties in the reflectance–SSA relationships (e.g. due to the crystal shape dependence) as seen by the large range (1.89–2.85) obtained by optimization.

α may also compensate for the influence of the grain shape in the microwave domain. This effect is difficult to quantify in the framework of the DMRT. In addition, as the grains at Dome C are mainly rounded or slightly faceted, we think this effect is of second order with respect to the above effects. However, the shape of the grain may be of greater importance in the Arctic where cup-like hoar is common.

Thus, several reasons may explain the value of α in the range 1.89–2.85, but it is difficult to take these effects into account and requires dedicated study. All the following analyses are presented considering the optimal value of α.

For the validity of the modeling, it is important to notice that despite the fact that $\alpha \sim 2$, the value of r/λ at 36.5 GHz ranges in average between 0.0650 and 0.075 over the first 1.6 m (i.e. about twice the penetration depth), and is lower than 0.05 at 18.7 GHz along the entire profile. The scaled grain-size profiles used to drive the radiative transfer model thus conform with the Rayleigh assumption (i.e. $r/\lambda < 0.159$).

Figure 3b shows the modeled brightness temperature with DMRT-ML driven by a scaled radius profile. For the three relationships, the modeled time series of brightness temperatures are significantly improved and have a magnitude similar to the observed time series. However, over the year, the brightness temperatures were slightly overestimated at 18.7 GHz, whereas they were underestimated at 36.5 GHz. These effects are stronger for ADC than for DC and KZ04.

The lowest mean rmse (1.41 K) was calculated for DC (Table 3). The largest difference, $T_B^{mod} - T_B^{amsre-e}$, was –2.9 K at 36.5 GHz in mid-September 2007 when the snowpack was warming. Another large difference, ~1.5–2.6 K, appeared in February 2007. At 18.7 GHz, the difference was usually close to 0.5 K during the first half of the year (until mid-June) and close to 1.4 K until mid-October; later the difference decreased to 0.5 K. Modeling results with KZ04 are similar, and the mean rmse is 1.54 K.

For ADC, brightness temperature at 18.7 GHz was strongly overestimated ($rmse_{18.7}$ = 3.60 K) and at 36.5 GHz was largely underestimated ($rmse_{36.5}$ = 2.95 K). For ADC only, errors at 18.7 GHz are larger than at 36.5 GHz (Table 3).

Nevertheless, the low rmse obtained with DC and KZ04 show that the brightness temperatures were improved compared with previous modeled results (Macelloni and others, 2007).

Using MEMLS and the KZ04 relationship, we obtained a scaling factor of 2.08. The time series were predicted with a mean rmse of 2.38 K, and most of this error was due to an overestimation of the modeled brightness temperatures during the summer. The quality of this result appears slightly lower than that obtained with DMRT-ML.

An interesting point to note is that by using an additional model the scaling factor obtained by optimization with MEMLS (2.08) was close to that found with DMRT-ML (1.89–2.85).

Sensitivity of the modeled brightness temperature to the snow grain size below 3 m depth

NIR photographs are available down to 3 m, but the 18.7 GHz channel has a penetration depth deeper than 3 m at Dome C (Sherjal and Fily, 1994; Macelloni and others, 2007; Picard and others, 2009b). It is worth noting that a constant grain size below 3 m depth is unrealistic. Nevertheless, such an assumption requires fewer unknowns than considering a more complex vertical profile of the grain size. To assess the influence of using a constant grain size below 3 m ($r^{z>3\,m}$), the sensitivity of this parameter was evaluated for the 18.7 GHz frequency. Figure 4 illustrates the large sensitivity of the modeled brightness temperature to the assumption

Downloaded from https://www.cambridge.org/core. 23 Nov 2021 at 12:30:57, subject to the Cambridge Core terms of use.

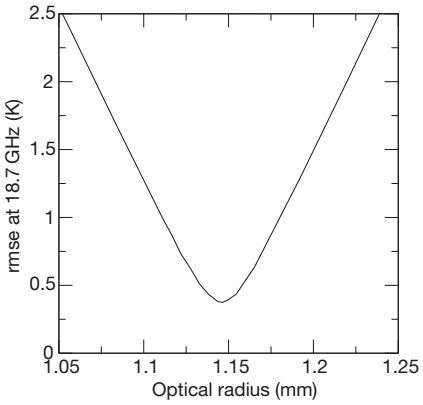


Fig. 4. The rmse at 18.7 GHz as a function of $r^{z>3m}$.

of a constant snow grain size below 3 m depth, while α is kept constant. To model brightness temperature at 18.7 GHz with an rmse lower than 0.5 K, $r^{z>3m}$ must be adjusted with an uncertainty lower than 0.03 mm. This analysis shows the lowest rmse accessible with a primary assumption. The value of $r^{z>3m}$ and the apparent sensitivity of the result to this value, are difficult to interpret. They should not be interpreted as the mean radius below 3 m depth. The reason is that the radiative transfer equation is nonlinear and many different profiles of grain size allow prediction of the observed brightness temperatures (Brucker, 2010).

From this finding, α and $r^{z>3m}$ are jointly estimated by minimizing the mean rmse (Equation (9)). For the three relationships, the scaling factor, α (Table 4), is lower than for the previous estimates shown in Table 3. The lower mean rmse values were predicted with $r^{z>3m}$ equal to 0.93, 1.14 and 0.80 mm for DC, ADC and KZ04, respectively. These effective radii are larger than those considered in the Methods section, where SSA = 9.8 m^2 kg^{-1}, i.e. $r^{z>3m}$ is 12–27% larger than the grain size measured at 3 m depth.

As a result, whatever the relationships used to convert reflectance to SSA, the time series of modeled brightness temperature show good agreement with the observations (Fig. 3c). The lowest mean rmse, 0.92 K (Table 4), is predicted for ADC, and the highest is 1.15 K for KZ04.

The amplitudes of the annual cycle, as well as the variations at shorter timescales, caused by rapid air-temperature changes, were accurately modeled at both frequencies. For instance, over July and August, the mean rmse for ADC is 0.46 and 0.53 K at 18.7 and 36.5 GHz, respectively. These errors are lower than the uncertainty of the AMSR-E sensor. In Figure 3c, the main disagreement appeared in summer (January to mid-February) and corresponds to an overestimated brightness temperature. This overestimation is present whatever the relationship used to derive the radius. A detailed analysis is presented below in 'Detailed analysis of the seasonal bias and the summer overestimation'.

It is worth noting that to achieve such a low rmse, the model needs to correctly predict the emissivity and the penetration depth at the two frequencies, i.e. four variables. Hence, even if two coefficients, α and $r^{z>3m}$, were optimized to obtain these results, the model and the profiles, in particular the value of the SSA measurements, significantly contribute to the quality of the results.

In the following, a validation of the grain-size gradient measured by NIR photography is presented. In order to evaluate the gradient of the SSA measurements using the NIR photography method, the grain-radius profile obtained using the ADC relationship is compared in Figure 5 with an idealized snow grain-size profile deduced using the method presented by Brucker and others (2010) for the pixel containing our snow pit measurements. First, the measured grain-size gradient over the top 3 m is in agreement with the gradient of the idealized profile (Brucker and others, 2010). This validation is independent of the α value. Second, the estimated $r^{z>3m}$ appears close to the idealized profile. Therefore, the estimated $r^{z>3m}$ does not dramatically change the entire grain-size gradient observed using NIR photography.

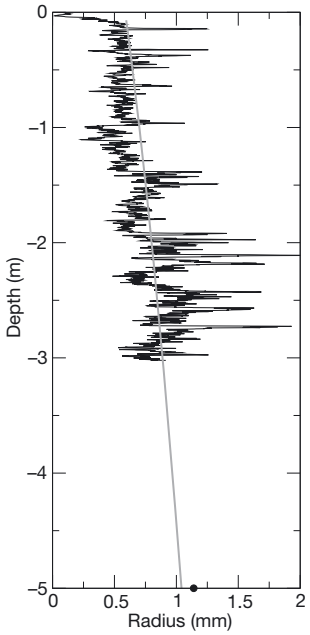


Fig. 5. Snow grain-size profiles obtained using the ADC relationship (black) and derived from Brucker and others (2010) (gray). The dot at 5 m depth corresponds to $r^{z>3m}$.

Validations in 2008 and 2009

The modeling with parameters optimized in 2007 was validated by predicting brightness temperatures for the period between January 2008 and March 2009. The validations were performed for the three relationships.

During the validation period, the amplitudes of the annual cycle were accurately predicted at both frequencies (Fig. 6) as well as the temperature variations in winter, in particular at 36.5 GHz. But, as shown in Figure 3c for 2007, the largest disagreement occurred in summer at 36.5 GHz with a maximum overestimation of 2.3 K.

A weak bias, corresponding to a temporal shift of 2 days, appeared during spring 2008. This may be explained by the assumption of a constant snow accumulation during the year.

Table 4. As Table 3, but using a joint estimate of α and $r^{z>3m}$

Relationship	α	$r^{z>3m}$	$rmse_{18.7}$	$rmse_{36.5}$	rmse
DC	2.44	0.93	0.36	1.46	1.06
ADC	2.71	1.14	0.32	1.26	0.92
KZ04	1.83	0.80	0.43	1.57	1.15

Downloaded from https://www.cambridge.org/core. 23 Nov 2021 at 12:30:57, subject to the Cambridge Core terms of use.

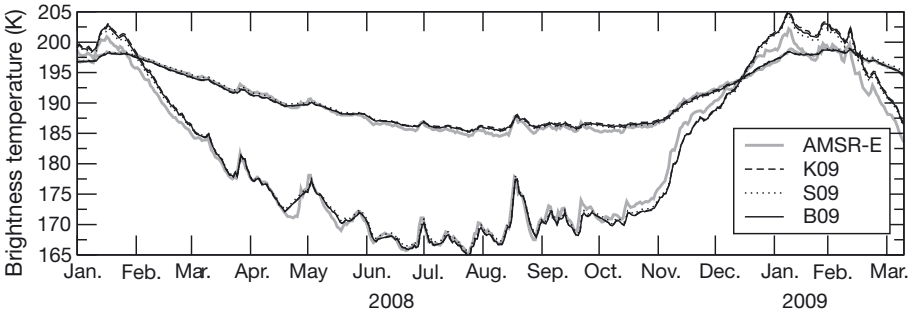


Fig. 6. Observed (gray curves) and modeled time series of vertically polarized brightness temperature at Dome C between January 2008 and March 2009 at 18.7 and 36.5 GHz using an optimized snow grain-size profile (i.e. α and $r^{z>3m}$ calibrated) for each relationship (DC, ADC and KZ04).

The seasonal bias between observed and modeled brightness temperatures is analyzed in detail in the next subsection.

The mean rmse calculated for 2008 was lower with ADC than with DC or KZ04, and equaled 0.77 K ($rmse_{18.7} = 0.39$ K and $rmse_{36.5} = 1.01$ K). Surprisingly, these results were slightly better in 2008 than in 2007 (mean rmse = 0.92 K).

Over the whole period, 2007–09 (27 months), the time series of brightness temperature at 18.7 and 36.5 GHz at vertical polarization were predicted with a mean rmse lower than 0.92 K. Owing to the accuracy of the AMSR-E radiometer, lower errors are in the range of uncertainties of the measurement, which are close to 0.7 K. The low values of rmse calculated here in 2008 are good, considering the assumption of constant profile of grain size. Indeed, density and NIR reflectance were measured in December 2006 and used throughout the period January 2007 to March 2009.

In order to better assess the quality of our results, and also to evaluate whether their comparison with only one AMSR-E pixel is adequate, we now analyze the spatial and temporal variability of the measured brightness temperature. The AMSR-E measurements for the pixel containing Dome C are compared with those surrounding the station. Indeed, it is worth noting that the satellite field-of-view dimensions of AMSR-E are (across- $\times$ along-track) 15 km $\times$ 25 km and 8 km $\times$ 14 km at 18.7 and 36.5 GHz, respectively, whereas the product used in this study has a 12.5 km $\times$ 12.5 km resolution.

Over the year 2008, the absolute mean annual difference between the pixel containing Dome C and the 3 $\times$ 4 pixels surrounding Dome C is 1.3 K at 18.7 GHz, and 1.0 K at 36.5 GHz. Macelloni and others (2007) provide a detailed analysis of the spatial variations in brightness temperature considering a larger area, 25 $\times$ 25 pixels, surrounding Dome C. The mean standard deviation of the difference between the observed time series over our field experiment and around it is <0.6 K at both 18.7 and 36.5 GHz. In addition, these standard deviation values remain the same in summer and in winter. Thus, the spatial variations in brightness temperature around Dome C, and the differences in the temporal evolutions, are weak. Using only the AMSR-E pixel containing the area of the in situ measurements is thus appropriate to compare with our modeling results.

Nevertheless, as mentioned earlier, daily-averaged brightness temperatures were used in this study. They result from several observations acquired (1) at different times and thus different near-surface temperatures and (2) from different positions of the satellite and thus with different viewing azimuth angles which make the measurements dependent on the surface roughness (Long and Drinkwater, 2000).

In order to consider these aspects, we analyzed the swath datasets (i.e. the 'AMSR-E/Aqua L2A Global Swath Spatially-Resampled Brightness Temperatures'). We quantified the inter-multipass variability with the averaged difference between the lowest and highest brightness temperature measured during the same day. The inter-multipass variability at 36.5 GHz (18.7 GHz) is 1.99 K (1.91 K) in summer, and 2.04 K (1.98 K) in winter. It is thus independent of the season (and thus of the near-surface temperature) and also of the frequency. We therefore conclude that the disagreement between the observed and modeled brightness temperatures present only in summer and only at 36.5 GHz result neither from an effect of the surrounding pixels nor from variations in the viewing azimuth angle.

Detailed analysis of the seasonal bias and the summer overestimation

Most of the error between observations and modeling results in Figures 3c and 7 is due to seasonal variations. In order to emphasize the weak seasonal bias, the modeled brightness temperatures were plotted as a function of observation for every day in 2007 and 2008 (Fig. 7).

At 36.5 GHz the biases in fall and spring were small and slightly different in 2007 and 2008 (Fig. 7b and d). In contrast, at 18.7 GHz, the bias was very small for both years (Fig. 7a and c).

In the range of depth from which the 36.5 GHz radiation emanates (typically 0.74–2 m in the East Antarctic plateau; Sherjal and Fily, 1994; Surdyk, 2002; Macelloni and others, 2007; Picard and others, 2009b), the vertical variation of the snow temperature is relatively significant with respect to the bias observed in Figure 7. For instance, the difference in snow temperature is ~2 K between 0.6 and 0.8 m depth. Hence, if the snow accumulation departs from the constant rate assumed, our calculation of the absolute depth of the probes may be shifted by a few centimeters. This assumption may produce the modeled seasonal bias.

Now, we focus on evaluating whether the summer overestimation in Figures 6 and 7b and d can be attributed to the atmospheric contribution to the top-of-atmosphere measured brightness temperatures. We ran simulations with the atmospheric radiative transfer model RTTOV driven by ECMWF ERA-40 reanalysis data. The objective of the following investigation is only to compare the atmospheric contributions to the brightness temperatures in summer vs winter.

Downloaded from https://www.cambridge.org/core. 23 Nov 2021 at 12:30:57, subject to the Cambridge Core terms of use.

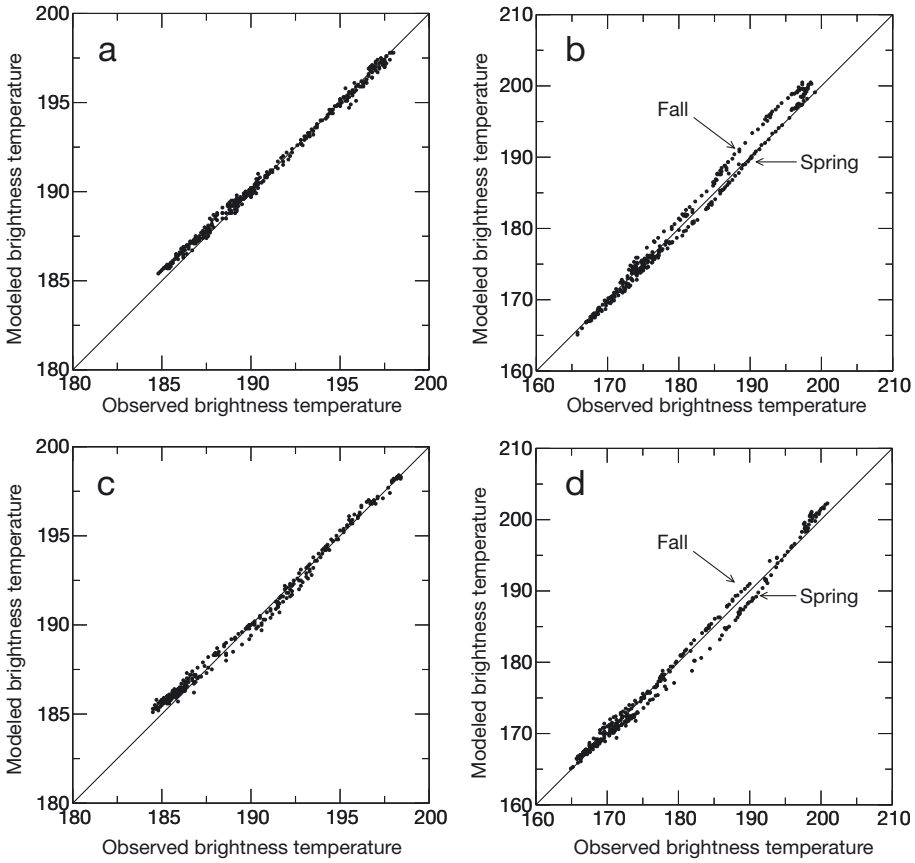


Fig. 7. Modeled vs observed brightness temperature during 2007 (a, b) and 2008 (c, d), at 18.7 GHz (a, c) and 36.5 GHz (b, d), using the ADC relationship.

At Dome C, top-of-atmosphere brightness temperatures were, all year round, higher than top-of-snowpack brightness temperatures by 2 K at 18.7 GHz and 1–5 K at 36.5 GHz. The most important point is that, at 36.5 GHz, the offset in winter (June–August) is ∼4.5 K, whereas in summer (December–February) it is ∼3.5 K. Thus, the offset between top-of-snowpack and top-of-atmosphere brightness temperature is higher in winter than in summer, which rules out using variations in atmospheric properties to explain the summer overestimation of modeled brightness temperatures. The main cause seems to be related to the constant snow grain size and density profiles assumed in our study.

Horizontally polarized brightness temperature

The model was run in 2007 using the three relationships (DC, ADC and KZ04) and parameters from Table 4. The modeled time series of horizontally polarized brightness temperature, at 36.5 GHz, are shown in Figure 8.

For the DC and KZ04 relationships, the magnitude of the modeled time series of brightness temperature was correctly predicted ($rmse_{36.5}$ is 2.01 K for DC and 2.07 K for KZ04). For ADC, the modeled brightness temperatures are systematically underestimated ($rmse_{36.5}$ is 2.97 K).

Most of the error comes from incorrect prediction of the rapid variations of brightness temperature (gray arrows in Fig. 8). This can be explained by our assumption of constant surface snow properties (e.g. the impact of surface hoar formation on brightness temperature was not considered; Shuman and Alley, 1993).

Brightness temperatures at 18.7 GHz (not shown) were predicted with a $rmse_{18.7}$ between 7.9 and 10.2 K, depending on the reflectance–SSA relationship used. These large errors are explained by the fact that the penetration depth at

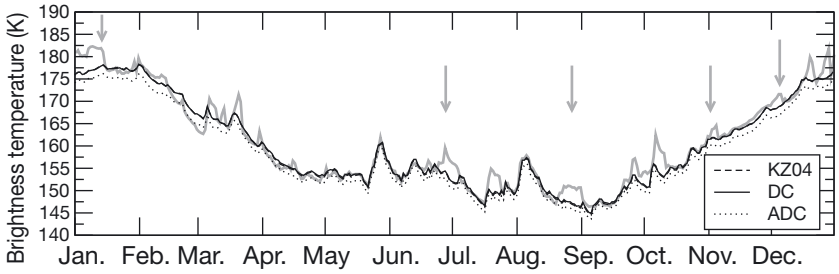


Fig. 8. Observed (gray curves) and modeled time series of horizontally polarized brightness temperature at Dome C in 2007 at 36.5 GHz using parameters in Table 4 and relationships DC, ADC and KZ04. The arrows indicate locations where a change in surface properties of the snowpack occurred.

Downloaded from https://www.cambridge.org/core. 23 Nov 2021 at 12:30:57, subject to the Cambridge Core terms of use.

18.7 GHz is 4.27–5.5 m (Sherjal and Fily, 1994; Macelloni and others, 2007), whereas the snow density profile was measured with a high vertical resolution only down to 3 m. Indeed, microwave observations are acquired at an incident angle where the surface reflection is weak at vertical polarization. However, this is not the case at horizontal polarization, which is thus more influenced by the vertical variations of snow density.

These modeling results indicate that density measurements below 3 m depth were too coarse to predict the horizontally polarized brightness temperature at 18.7 GHz.

CONCLUSIONS

A 2 year long time series of vertically polarized brightness temperatures, at 18.7 and 36.5 GHz at Dome C, was predicted using a multilayer electromagnetic model (DMRT-ML) driven by new snow measurements of temperature, density and grain size. The main novelty was to derive the snow grain-size profile from vertical NIR photographs of a snow pit wall. The optical radius profile was measured down to 3 m depth with a millimeter-scale vertical resolution. Three relationships were tested to convert the vertical NIR reflectance profile into SSA and then into radius profile. The empirical relationship, ADC, based on the largest number of measurements, was slightly better and allowed more accurate modeling results.

As a first step, the snow grain size below 3 m depth was kept constant at the only available measurements (at 4 m depth). Considering the radius profile without any adjustment, results show a large overestimation of brightness temperatures (rmse $\simeq$ 28 K).

For the second step, the radius profile was multiplied by a constant factor of 1.89–2.85. Results were significantly improved (rmse $\simeq$ 1.5 K), which demonstrates that SSA derived from NIR photography is able to provide profiles adequate for microwave modeling if a scaling factor is applied. We gave a qualitative explanation for this scaling factor, but further work is needed to precisely specify the link between SSA and radius in the DMRT.

At the third step, the sensitivity of the snow grain size below 3 m depth was evaluated. With a calibrated scaling factor and a snow grain size below 3 m depth, brightness temperatures were further slightly improved (rmse $\simeq$ 1 K) for all the relationships relating NIR reflectance to SSA. Modeled brightness temperatures at 18.7 GHz present a large sensitivity to grain size below 3 m depth, which emphasizes the need for deep SSA measurements.

We conclude from these simulations that highly resolved vertical profiles of grain size are necessary to model brightness temperatures. To extend this study to the lower frequencies available on AMSR-E (6.9 and 10.7 GHz) much deeper profiles (>10 m) are needed, which cannot be obtained by NIR photography in snow pits.

Furthermore, despite the fact that the spatial variation of brightness temperature measured at Dome C by satellite is weak, a single snow pit may not be representative of the Dome C area at the microwave pixel scale.

In future work, more complex models can be used to consider (1) the various shapes of snow grains, through the stickiness factor; (2) a parameterization of scattering based on the Mie theory, rather than the Rayleigh assumption in the DMRT; and (3) a distribution of grain size in each snow layer. However, these parameterizations require additional variables that are not easy to measure.

ACKNOWLEDGEMENTS

This work was supported by the French remote-sensing program (Programme National de Télédétection Spatiale), the programs INSU-CNRS (LEFE NIEVE and Méso équipement Glacio Concordia) and the project of the Agence Nationale de la Recherche (ANR-07-VULN-013 VANISH). We thank Centre National d'Etudes Spatiales (CNES) for funding for the program API-THORPEX-CONCORDIASI and the French polar institute, IPEV, for logistical support. M.S. was supported by a grant from SATW 'Germaine de Staël'.

REFERENCES

Arnaud, L., M. Gay, J.-M. Barnola and P. Duval. 1998. Imaging of firn and bubbly ice in coaxial reflected light: a new technique for the characterization of these porous media. *J. Glaciol.*, **44**(147), 326–332.

Barnola, J.-M., R. Pierritz, C. Goujon, P. Duval and E. Boller. 2004. 3D reconstruction of the Vostok firn structure by X-ray tomography. *Mater. Glyatsiol. Issled./Data Glaciol. Stud.* 97. 80–84.

Brandt, R.E. and S.G. Warren. 1997. Temperature measurements and heat transfer in near-surface snow at the South Pole. *J. Glaciol.*, **43**(144), 339–351.

Brucker, L. 2010. Modélisation de l'émission micro-onde du manteau neigeux: applications en Antarctique et au Québec. (PhD thesis, Université Joseph Fourier.)

Brucker, L., G. Picard and M. Fily. 2010. Snow grain-size profiles deduced from microwave snow emissivities in Antarctica. *J. Glaciol.*, **56**(197), 514–526.

Brunjail, H., L. Arnaud, M. Schneebeli, J.-M. Barnola and P. Duval. 2009. Micro-structure de la neige et du névé à Dome Concordia. Grenoble, Université Joseph Fourier, Laboratoire de Glaciologie et Géophysique de l'Environnement. (Technical Report.)

Chen, C.T., L. Tsang, J. Guo, A.T.C. Chang and K.-H. Ding. 2003. Frequency dependence of scattering and extinction of dense media based on three-dimensional simulations of Maxwell's equations with applications to snow. *IEEE Trans. Geosci. Remote Sens.*, **41**(8), 1844–1852.

Colbeck, S.C. *and 7 others*. 1990. *The international classification for seasonal snow on the ground*. Wallingford, Oxon, International Association of Scientific Hydrology. International Commission on Scnow and Ice.

Davis, R.E., J. Dozier and R. Perla. 1987. Measurement of snow grain properties. *In* Jones, H.G. and W.J. Orville-Thomas, *eds. Seasonal snowcovers: physics, chemistry, hydrology*. Dordrecht, etc., D. Reidel Publishing Co., 63–74.

Debye, P., H.R. Anderson and H. Brumberger. 1957. Scattering by an inhomogeneous solid II. The correlation function and its application. *J. Appl. Phys.*, **28**(6), 679–683.

Domine, F., A. Cabanes, A.S. Taillandier and L. Legagneux. 2001. Specific surface area of snow samples determined by CH_4 adsorption at 77 K and estimated by optical microscopy and scanning electron microscopy. *Environ. Sci. Technol.*, **35**(4), 771–780.

Domine, F., R. Salvatori, L. Legagneux, R. Salzano, M. Fily and R. Casacchia. 2006. Correlation between the specific surface area and the short wave infrared (SWIR) reflectance of snow. *Cold Reg. Sci. Technol.*, **46**(1), 60–68.

Flin, F., J.B. Brzoska, B. Lesaffre, C. Coléou and R.A. Pieritz. 2003. Full three-dimensional modelling of curvature-dependent snow metamorphism: first results and comparison with experimental tomographic data. *J. Phys. D*, **36**(10A), A49–A54.

Downloaded from https://www.cambridge.org/core. 23 Nov 2021 at 12:30:57, subject to the Cambridge Core terms of use.

Gallet, J.-C., F. Domine, C.S. Zender and G. Picard. 2009. Measurement of the specific surface area of snow using infrared reflectance in an integrating sphere at 1310 and 1550 nm. *Cryosphere*, **3**(2), 167–182.

Gallet, J.-C., F. Domine, L. Arnaud, G. Picard and J. Savarino. 2010. Vertical profiles of the specific surface area of the snow at Dome C, Antarctica. *Cryos. Discuss.*, **4**(3), 1647–1708.

Giddings, J.C. and E. LaChapelle. 1961. Diffusion theory applied to radiant energy distribution and albedo of snow. *J. Geophys. Res.*, **66**(1), 181–189.

Grenfell, T.C. and S.G. Warren. 1999. Representation of a nonspherical ice particle by a collection of independent spheres for scattering and absorption of radiation. *J. Geophys. Res.*, **104**(D24), 31,697–31,709.

Grody, N. 2008. Relationship between snow parameters and microwave satellite measurements: theory compared with Advanced Microwave Sounding Unit observations from 23 to 150 GHz. *J. Geophys. Res.*, **113**(D22), D22108. (10.1029/2007JD009685.)

Jin, Y.-Q. 1993. *Electromagnetic scattering modelling for quantitative remote sensing*. Singapore, World Scientific.

Kerbrat, M., B. Pinzer, T. Huthwelker, H.W. Gäggeler, M. Ammann and M. Schneebeli. 2008. Measuring the specific surface area of snow with X-ray tomography and gas adsorption: comparison and implications for surface smoothness. *Atmos. Chem. Phys.*, **8**(5), 1261–1275.

Kokhanovsky, A.A. and E.P. Zege. 2004. Scattering optics of snow. *Appl. Opt.*, **43**(7), 1589–1602.

Lagarias, J.C., J.A. Reeds, M.H. Wright and P.E. Wright. 1998. Convergence properties of the Nelder–Mead simplex method in low dimensions. *SIAM J. Opt.*, **9**(1), 112–147.

Langlois, A. *and 8 others*. 2010. On the relationship between snow grain morphology and *in-situ* near infrared calibrated reflectance photographs. *Cold Reg. Sci. Technol.*, **61**(1), 34–42.

Legagneux, L., A. Cabanes and F. Domine. 2002. Measurement of the specific surface area of 176 snow samples using methane adsorption at 77 K. *J. Geophys. Res.*, **107**(D17), 4335. (10.1029/2001JD001016.)

Lemmetyinen, J. *and 9 others*. 2009. A comparison of airborne microwave brightness temperatures and snowpack properties across the boreal forests of Finland and Western Canada. *IEEE Trans. Geosci. Remote Sens.*, **47**(3), 965–978.

Liang, D., K. Tse, Y. Tan, L. Tsang and K.H. Ding. 2006. Scattering and emission in snow based on QCA/DMRT and numerical Maxwell model of 3Dimensional simulations (NMM3D). *In Proceedings of the IEEE 9th Specialist Meeting on Microwave Radiometry and Remote Sensing of the Environment (MicroRad 2006), 28 February–3 March 2006, San Juan, Puerto Rico*. Piscataway, NJ, Institute of Electrical and Electronics Engineers, 197–202.

Liang, D., X. Xu, L. Tsang, K.M. Andreadis and E.G. Josberger. 2007. Modeling multi-layer effects in passive microwave remote sensing of dry snow using Dense Media Radiative Transfer Theory (DMRT) based on quasicrystalline approximation. *In Proceedings of International Geoscience and Remote Sensing Symposium (IGARSS 2007), 23–28 July, 2007, Barcelona, Spain*. Piscataway, NJ, Institute of Electrical and Electronics Engineers, 1215–1218.

Liang, D., X. Xu, L. Tsang, K.M. Andreadis and E.G. Josberger. 2008. The effects of layers in dry snow on its passive microwave emissions using dense media radiative transfer theory based on the quasicrystalline approximation (QCA/DMRT). *IEEE Trans. Geosci. Remote Sens.*, **46**(11), 3663–3671.

Long, D.G. and M.R. Drinkwater. 2000. Azimuth variation in microwave scatterometer and radiometer data over Antarctica. *IEEE Trans. Geosci. Remote Sens.*, **38**(4), 1857–1870.

Macelloni, G., S. Paloscia, P. Pampaloni and M. Tedesco. 2001. Microwave emission from dry snow: a comparison of experimental and model results. *IEEE Trans. Geosci. Remote Sens.*, **39**(12), 2649–2656.

Macelloni, G., M. Brogioni, P. Pampaloni and A. Cagnati. 2007. Multifrequency microwave emission from the Dome-C area on the east Antarctic plateau: temporal and spatial variability. *IEEE Trans. Geosci. Remote Sens.*, **45**(7), 2029–2039.

Matzl, M. and M. Schneebeli. 2006. Measuring specific surface area of snow by near-infrared photography. *J. Glaciol.*, **52**(179), 558–564.

Matzl, M. and M. Schneebeli. 2010. Stereological measurement of the specific surface area of seasonal snow types: comparison to other methods, and implications for mm-scale vertical profiling. *Cold Reg. Sci. Technol.*, **64**(1), 1–8.

Mätzler, C. 1998. Improved Born approximation for scattering in a granular medium. *J. Appl. Phys.*, **83**(11), 6111–6117.

Mätzler, C. 2002. Relation between grain-size and correlation length of snow. *J. Glaciol.*, **48**(162), 461–466.

Mätzler, C. and A. Wiesmann. 1999. Extension of the microwave emission model of layered snowpacks to coarse-grained snow. *Remote Sens. Environ.*, **70**(3), 317–325.

Mounirou Toure, A., K. Goïta, A. Royer, C. Mätzler and M. Schneebeli. 2008. Near-infrared digital photography to estimate snow correlation length for microwave emission modeling. *Appl. Opt.*, **47**(36), 6723–6733.

Painter, T.H., N.P. Molotch, M. Cassidy, M. Flanner and K. Steffen. 2007. Contact spectroscopy for determination of stratigraphy of snow optical grain size. *J. Glaciol.*, **53**(180), 121–127.

Perla, R.I., J. Dozier and R.E. Davis. 1986. Preparation of serial sections in dry snow specimens. *J. Microsc.*, **141**, 111–114.

Picard, G., L. Arnaud, F. Domine and M. Fily. 2009a. Determining snow specific surface area from near-infrared reflectance measurements: numerical study of the influence of grain shape. *Cold Reg. Sci. Technol.*, **56**(1), 10–17.

Picard, G., L. Brucker, M. Fily, H. Gallée and G. Krinner. 2009b. Modeling time series of microwave brightness temperature in Antarctica. *J. Glaciol.*, **55**(191), 537–551.

Pulliainen, J.T., J. Grandell and M.T. Hallikainen. 1999. HUT snow emission model and its applicability to snow water equivalent retrieval. *IEEE Trans. Geosci. Remote Sens.*, **37**(3), 1378–1390.

Rosenkranz, P.W. 1992. Rough-sea microwave emissivities measured with the SSM/I. *IEEE Trans. Geosci. Remote Sens.*, **30**(5), 1081–1085.

Saunders, R., M. Matricardi and P. Brunel. 1999. An improved fast radiative transfer model for assimilation of satellite radiance observations. *Q. J. R. Meteorol. Soc.*, **125**(556), 1407–1425.

Sherjal, I. and M. Fily. 1994. Temporal variations of microwave brightness temperatures over Antarctica. *Ann. Glaciol.*, **20**, 19–25.

Shuman, C.A. and R.B. Alley. 1993. Spatial and temporal characterization of hoar formation in central Greenland using SSM/I brightness temperatures. *Geophys. Res. Lett.*, **20**(23), 2643–2646.

Steig, E.J., D.P. Schneider, S.D. Rutherford, M.E. Mann, J.C. Comiso and D.T. Shindell. 2009. Warming of the Antarctic ice-sheet surface since the 1957 International Geophysical Year. *Nature*, **457**(7228), 459–462.

Surdyk, S. 2002. Using microwave brightness temperature to detect short-term surface air temperature changes in Antarctica: an analytical approach. *Remote Sens. Environ.*, **80**(2), 256–271.

Tedesco, M. and E.J. Kim. 2006. Intercomparison of electromagnetic models for passive microwave remote sensing of snow. *IEEE Trans. Geosci. Remote Sens.*, **44**(10), 2654–2666.

Tedesco, M. *and 7 others*. 2006. Comparison of local scale measured and modelled brightness temperatures and snow parameters from the CLPX 2003 by means of a dense medium radiative transfer theory model. *Hydrol. Process.*, **20**(4), 657–672.

Tsang, L. and J.A. Kong. 2001. *Scattering of electromagnetic waves: advanced topics*. New York, Wiley.

Tsang, L., C.T. Chen, A.T.C. Chang, J. Guo and K.H. Ding. 2000. Dense media radiative transfer theory based on quasicrystalline approximation with application to passive microwave remote sensing of new snow. *Radio Sci.*, **35**(3), 731–749.

Downloaded from https://www.cambridge.org/core. 23 Nov 2021 at 12:30:57, subject to the Cambridge Core terms of use.

Tsang, L., J. Pan, D. Liang, Z. Li, D.W. Cline and T. Tan. 2007. Modeling active microwave remote sensing of snow using dense media radiative transfer (DMRT) theory with multiple-scattering effects. *IEEE Trans. Geosci. Remote Sens.*, **45**(4), 990–1004.

Tsang, L., D. Liang, X. Xu and P. Xu. 2008. Microwave emission from snowpacks: modeling the effects of volume scattering, surface scattering and layering. *In Proceedings of 10th Specialist Meeting on Microwave Radiometry and Remote Sensing of the Environment (MicroRad 2008), 11–14 March 2008, Firenze, Italy*. Piscataway, NJ, Institute of Electrical and Electronics Engineers, 1–4.

Tse, K.K., L. Tsang, C.H. Chan, K.H. Ding and K.W. Leung. 2007. Multiple scattering of waves by dense random distributions of sticky particles for applications in microwave scattering by terrestrial snow. *Radio Sci.*, **42**(RS5), RS5001. (10.1029/2006RS003476.)

Turner, J. *and 8 others*. 2005. Antarctic climate change during the last 50 years. *Int. J. Climatol.*, **25**(3), 279–294.

Uppala, S.M. *and 45 others*. 2005. The ERA-40 re-analysis. *Q. J. R. Meteorol. Soc.*, **131**(612), 2961–3212.

Urbini, S. *and 6 others*. 2008. Historical behaviour of Dome C and Talos Dome (East Antarctica) as investigated by snow accumulation and ice velocity measurements. *Global Planet. Change*, **60**(3–4), 576–588.

Warren, S.G. and R.E. Brandt. 2008. Optical constants of ice from the ultraviolet to the microwave: a revised compilation. *J. Geophys. Res.*, **113**(D14), D14220. (10.1029/2007JD009744.)

West, R., L. Tsang and P. Winebrenner. 1993. Dense medium radiative transfer theory for two scattering layers with a Rayleigh distribution of particle sizes. *IEEE Trans. Geosci. Remote Sens.*, **31**(2), 426–437.

Wiesmann, A. and C. Mätzler. 1999. Microwave emission model of layered snowpacks. *Remote Sens. Environ.*, **70**(3), 307–316.

Wiesmann, A., C. Mätzler and T. Weise. 1998. Radiometric and structural measurements of snow samples. *Radio Sci.*, **33**(2), 273–289.

Zwally, H.J. 1977. Microwave emissivity and accumulation rate of polar firn. *J. Glaciol.*, **18**(79), 195–215.

MS received 31 July 2009 and accepted in revised form 14 October 2010

Downloaded from https://www.cambridge.org/core. 23 Nov 2021 at 12:30:57, subject to the Cambridge Core terms of use.